Coherence Analysis Estimation For Event Detection

Abdul Hafiz S Issah[1,2] & Eileen R Martin[1,2,3,4]

[1]*Center for Wave Phenomena,* [2]*Department of Applied Math and Statistics,* [3]*Department of Geophysics,* [4]*Hydrologic Science and Engineering Program*
Colorado School of Mines, Golden CO 80401
email: aissah@mines.edu

ABSTRACT

As large-scale passive data are collected more frequently, we need tools that can more quickly help us explore possible seismic events in massive seismic data. This paper presents a new algorithm that uses QR decomposition as a proxy for event detection in seismic data through coherence analysis. The algorithm requires identified events to exhibit coherence between sensors across multiple sub-windows or transient high amplitudes. By employing the QR decomposition, the algorithm streamlines the computation process, enhancing its applicability in real-time event identification scenarios or improving user interactivity during large-scale data exploration. e show that two key steps in the typical coherence analysis workflow (i.e. matrix-matrix multiplication and eigenvalue decomposition) can be condensed into a single step through our use of the QR decomposition. This results in a faster algorithm. Experimental results demonstrate the algorithm's effectiveness in distinguishing seismic events from background noise, showcasing its potential for practical implementation in seismic monitoring systems.

Key words: Event Detection, Coherence, Numerical Linear Algebra, DAS

1 INTRODUCTION

As seismic instrumentation advances, multiple techniques for detecting and characterizing events have emerged. These include methods such as Short-Term Average/Long-Term Average (STA/LTA), which rely on amplitude changes, and template matching, which necessitates pre-existing event templates for identification ((Gibbons and Ringdal, 2006), (Sabbione and Velis, 2010)). These methods have drawbacks, either in terms of limited applicability to noisy data, or significant computational cost. Coherence-based methods detect events by exploiting the similarity of recorded events on adjacent sensors. With the increasing prevalence of dense recording systems like Distributed Acoustic Sensing (DAS), coherence-based methods offer a promising alternative, particularly when conventional methods prove ineffective.

Coherence-based methods can be used as a way to measure how similar time series recorded by neighboring sensors are, serving as an indicator for event occurrences. However, a drawback of this approach is its reliance on parameters such as array spacing to differentiate between coherent events and noise. Therefore, it becomes imperative to carefully select these parameters based on the targeted events. Seydoux et al. (2016) found that covariance matrices, a closely related technique to the one used in this report, can effectively identify teleseismic earthquakes and seismic activity from local sources contingent upon the chosen parameters. When applying these methodologies to DAS data, we have the flexibility to adjust sensor spacing during processing, considering the frequency range of the events of interest and the potential noise levels, thereby mitigating the risk of false detections.

Our research interest here comprises exploring efficient methods for event detection through coherence analysis, coupled with compression techniques that enable us to achieve this with minimal data transfer. In this report, we talk about a fast estimation algorithm and its connection with the conventional approach to coherence analysis. We first describe the traditional implementation of coherence analysis for an array of sensors, followed by an exploration of QR decomposition and its potential to streamline computations. Our findings indicate that two of the steps in the process of coherence matrix analysis —matrix-matrix multiplication and eigenvalue decomposition—can be condensed into a single step by employing QR decomposition resulting in a new, faster algorithm. This streamlined approach for detection estimation shows effectiveness that is comparable to the conventional method. We conduct a computational time comparison between these methods to assess their efficacy.

2 THEORY

COHERENCE ANALYSIS

Coherence analysis is a statistical tool that can be used for evaluating the similarity between two signals. It quantifies the degree of correlation between signals, with a coherence value of 1 indicating a strong positive correlation, -1 indicating a strong negative correlation, and values in between reflecting the extent of correlation. For an array of n sensors each recording a time series, a coherence matrix at any frequency, f, can be constructed which has entries representing the coherence between pairs of signals. For example, the i^{th} entry of the j^{th} column of the coherence matrix would correspond to the coherence of the signal recorded by sensor number i with the signal recorded by sensor number j. The covariance matrix, another commonly employed matrix, differs by its absence of a normalization factor, resulting in a range spanning from ∞ to $-\infty$. The use of these matrices in event detection originates from Lawley (1956), which proposes that the eigenvalues of coherence matrices correspond to the sizes of independent signals within the data. In seismic data analysis, the largest eigenvalues typically represent the coherent signals, whereas the smaller ones often correspond to background noise (Seydoux et al., 2016).

The coherence of two signals, x, and y can be computed at frequency, f as

$$C_{x,y}(f) = \frac{|E[P_{x,y}(f)]|^2}{E[P_{x,x}(f)]E[P_{y,y}(f)]} \tag{1}$$

where $P_{x,y}(f)$ is the cross-spectral density between $x(t)$ and $y(t)$ at frequency, f, while $P_{x,x}(f)$ and $P_{y,y}(f)$ represent the auto-spectral density of $x(t)$ and $y(t)$, respectively. The spectral densities are defined as:

$$P_{x,y}(f) = \mathcal{F}_x(f)\overline{\mathcal{F}_y(f)} \qquad P_{x,x}(f) = \mathcal{F}_x(f)\overline{\mathcal{F}_x(f)} \qquad P_{y,y}(f) = \mathcal{F}_y(f)\overline{\mathcal{F}_y(f)}$$

where $\mathcal{F}_x(f)$ and $\mathcal{F}_y(f)$ represent the Fourier transform of x and y at frequency f and $\bar{\cdot}$ refers to the complex conjugate operation. In certain applications, coherence analysis aims to assess the similarity between two signals that do not have a previously well-understood relationship, such as in studying the relationship between electroencephalogram (EEG) and electromyogram (EMG) signals to understand the connection between the brain and muscles (Coffey et al., 2021). In those cases, we need a statistically sufficient number of samples to achieve reliable estimations. However, when detecting seismic events, our focus lies in identifying short-term coherence between offset signals that should appear somewhat similarly on nearby sensors. As a result, we can achieve the desired results by finding the average within small averaging windows. In such scenarios, we can use the Welch's method within each averaging window:

$$C_{x,y}(f) = \frac{|\sum_{i=1}^{n} P_{x,y}^{(i)}(f)|^2}{\sum_{i=1}^{n} P_{x,x}^{(i)}(f) \sum_{i=1}^{n} P_{y,y}^{(i)}(f)} = \frac{\left|\sum_{i=1}^{n} \mathcal{F}_x^{(i)}(f)\overline{\mathcal{F}_y^{(i)}(f)}\right|^2}{\sum_{i=1}^{n} \mathcal{F}_x^{(i)}(f)\overline{\mathcal{F}_x^{(i)}(f)} \sum_{i=1}^{n} \mathcal{F}_y^{(i)}(f)\overline{\mathcal{F}_y}} \tag{2}$$

Where n is the number of sub-windows within the averaging window. Hence, for each sub-window, we need the Fourier transform value at frequency, f for x and y, that is, $\mathcal{F}_x^{(i)}(f)$ and $\mathcal{F}_y^{(i)}(f)$. Letting

$$U_f^{(i)}(x) = \frac{\mathcal{F}_x^{(i)}(f)}{(\sum_{i=1}^{n} \mathcal{F}_x^{(i)}(f)\overline{\mathcal{F}_x^{(i)}(f)} \sum_{i=1}^{n} \mathcal{F}_y^{(i)}(f)\overline{\mathcal{F}_y})^{\frac{1}{4}}} \qquad \text{and} \qquad U_f^{(i)}(y) = \frac{\mathcal{F}_y^{(i)}(f)}{(\sum_{i=1}^{n} \mathcal{F}_x^{(i)}(f)\overline{\mathcal{F}_x^{(i)}(f)} \sum_{i=1}^{n} \mathcal{F}_y^{(i)}(f)\overline{\mathcal{F}_y})^{\frac{1}{4}}}$$

then,

$$C_{x,y}(f) = \left|\sum_{i=1}^{n} U_f^{(i)}(x)\overline{U_f^{(i)}(y)}\right|^2 \tag{3}$$

The coherence matrix can be constructed as,

$$C(f) = \begin{bmatrix} C_{x,y}(f) & C_{x,y}(f) \\ C_{y,x}(f) & C_{y,y}(f) \end{bmatrix} = \left|\sum_{i=1}^{n} U_f^{(i)}\overline{U_f^{(i)}}^T\right|^2 = \left|U_f\overline{U_f}^T\right|^2$$

where,

$$U_f^{(i)} = \begin{bmatrix} U_f^{(i)}(x) \\ U_f^{(i)}(y) \end{bmatrix} \qquad \text{and} \qquad U_f = \begin{bmatrix} U_f^{(1)}(x) & U_f^{(2)}(x) & \dots & U_f^{(n)}(x) \\ U_f^{(1)}(y) & U_f^{(2)}(y) & \dots & U_f^{(n)}(y) \end{bmatrix}$$

Hence for an array of s sensors,

$$C(f) = \left|U_f U_f^H\right|^2 \tag{4}$$

Where,

$$U_f = \begin{bmatrix} U_f^{(1)}(1) & U_f^{(2)}(1) & \dots & U_f^{(n)}(1) \\ U_f^{(1)}(2) & U_f^{(2)}(2) & \dots & U_f^{(n)}(2) \\ \vdots & \vdots & \ddots & \vdots \\ U_f^{(1)}(s) & U_f^{(2)}(s) & \dots & U_f^{(n)}(s) \end{bmatrix} \tag{5}$$

H is the hermitian operator, and $|.|^2$ is applied element-wise to construct $C(f)$.

Using a coherence matrix for event detection

After the computation of the coherence matrix, we use it as an event detection tool by finding and studying the decay of the eigenvalues of the coherence matrix. If a few eigenvalues significantly surpass others by orders of magnitude, we attribute them to individual events. Conversely, if the eigenvalues exhibit comparable magnitudes, they predominantly signify background noise. There are various ways of quantifying this with a detection parameter. In this report, we use,

$$\text{detection parameter} = \frac{\lambda_1}{\sum_{i=1}^{n} \lambda_i} \tag{6}$$

Where λ_k is the kth eigenvalue when the eigenvalues are ordered by magnitude. In this case, once we set a threshold, we can classify whether or not there is one significant event.
In summary, we carry out the following steps for event detection to each averaging window separately.

(i) Divide the averaging window into w sub-windows.
(ii) For each sub-window, (i),

- Compute the Discrete Fourier Transform for each sensor, x
- Use the Fourier transform value corresponding to frequency f to compute $U_f^{(i)}(x)$

(iii) Use the computed values to build the matrix, U_f.
(iv) Using eigenvalue decomposition of $C(f) = \left|U_f U_f^H\right|^2$, compute the detection parameter.
(v) Choosing a threshold, use detection parameter to classify events and background noise

This report is focused primarily on finding a more efficient approximation than this standard technique, but that also maintains sufficient accuracy for practical applications.

QR Decomposition

The QR decomposition factors a matrix into two constituent matrices: a unitary matrix, Q, and an upper triangular matrix, R. In this decomposition, the columns of Q embody a set of orthogonal directions that capture all the information within the original matrix. The entries of R represent the proportion of each of the columns in Q contained in the columns of the original matrix. Specifically, the i^{th} entry of the j^{th} row of the R matrix represents the magnitude of the j^{th} column of the Q matrix contained in the i^{th} column of the original matrix. The Q matrix can be constructed by choosing one column of the original matrix, and then finding other directions in the original matrix perpendicular to this direction.
When finding the eigenvalue decomposition of $C(f)$, we want to find a unitary matrix of eigenvectors, Λ and a diagonal matrix of eigenvalues, D such that,

$$C(f) = \Lambda D \Lambda^T \tag{7}$$

We propose that if the columns of Q approximate the direction pointed to by the eigenvectors of $C(f)$, we can approximate $C(f)$ as:

$$C(f) \approx Q \tilde{D} Q^T \tag{8}$$

Let,

$$U_f = QR$$

Then,

$$\begin{aligned} C(f) &= \left| U_f U_f^H \right|^2 \\ &= \left| QR(QR)^H \right|^2 \\ &= \left| QRR^H Q^H \right|^2 \\ &= QRR^H Q^H QRR^H Q^H \end{aligned}$$

Since Q is unitary, $Q^H Q = \mathbf{I}$. This gives,

$$\begin{aligned} C(f) &= QRR^H RR^H Q^H \\ &= Q \left| RR^H \right|^2 Q^H \end{aligned}$$

Comparing this with equation 8 gives,

$$Q \left| RR^H \right|^2 Q^H \approx Q\tilde{D}Q^T$$

So now assuming that RR^H is approximately diagonal, the eigenvalues of the coherence matrix can be approximated by the diagonal of RR^H. That is,

$$\tilde{D} \approx diag(\left| RR^H \right|^2) = diag(RR^H)^2$$

Through computational experiments, we realized that $diag(RR^H)$ works as well as $diag(RR^H)^2$ and produces results closer to the traditional methods. Hence, we use $diag(RR^H)$ in our algorithm.

Computational comparison

Using random matrices, we explore the computational efficiency of the proposed algorithm in comparison to two other techniques of calculating the exact or approximate eigenvalues of the coherence matrix. The matrices used here have a column dimension half the size of the row dimension, reflecting the anticipated scenario in the case of streaming DAS data where there are more sensors (rows) than time sub-windows (columns). The random matrix here is analogous to U_f as used in computing $C(f)$ above. We compute the eigenvalues as we would in the traditional method. Then we approximate the eigenvalues using our algorithm -which uses the QR decomposition- and by using the square of the singular values of U_f. The results of this test are summarized in Figure 1. The x axis shows the number of rows in the random matrix versus the computation time on the y axis. Traditional computation methods exhibit the longest processing times, followed by an SVD-related approach. Conversely, the new QR-based approach demonstrates the shortest processing time.

3 EXPERIMENTS

DATA

The data used in our computational experiments here was recorded in 2016 at the Brady Hot Springs site in Nevada as part of an investigation into the feasibility of using Distributed Acoustic Sensing (DAS) for cost-effective monitoring of geothermal reservoirs. The data consists of approximately 8km of fiber optic cable deployed horizontally in a shallow trench, with 1m channel spacing resulting in around 8000 channels recording at 1000 samples per second (Coleman, 2016).

In choosing data to test our algorithm on, we select snapshots of data from the Brady Hot Springs dataset that provide anticipated responses for both events and background noise when subjected to coherence analysis. For the background noise, we use data recorded between 12:00:18 AM and 12:01:18 AM on March 12, 2016, as shown in 2 (bottom). For microseismic event data, we use data recorded between 8:38:18 AM and 8:39:28 AM on March 14, 2016, shown in 2 (top). This data contains three microseismic events that happen within the space of about five seconds from each other according to the event catalog provided by Li and Zhan (2018). The selected channels are chosen from a linear part of the array from channels 3100 to 5100.

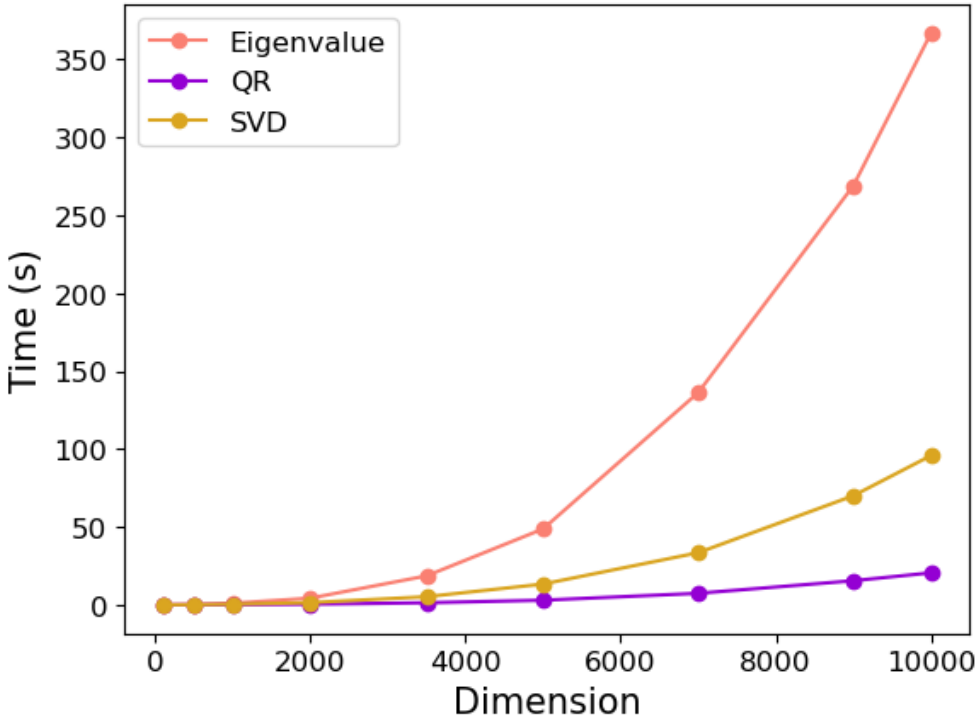

Figure 1. Computational test for the efficiency of the proposed algorithm in comparison to other alternatives. The data used are random matrices of size dimension rows by 0.5*dimensions columns.

Test of coherence for detection

From the data described above, we select 200 sensors at a regular interval of about 10m, and using a sub-window length of five seconds and no overlap between sub-windows, we compute the detection parameter at the various frequencies using the traditional coherence analysis approach. This result is summarized in figure 3. The detection parameters for the background noise are depicted in yellow, whereas those for the microseismic events are represented in violet. It's notable that the background noise curve exhibits a predominantly flat profile, with the exception of a few spikes. One particularly significant spike occurs at 7.5 Hz, which is also prominently visible in the events curve. This spike likely arises from a consistent noise source present across the whole dataset. Conversely, the event curve shows high values within a wider frequency range below 50 Hz, which peaks around 20 Hz. Our goal is to make similar plots with distinctive noise and event profiles using a more efficient algorithm.

Next, we redo the same computational experiment using the method of QR approximation outlined above. The result of this test shown in figure 4 shows a similar pattern as seen in figure 3. This pattern indicates a clear distinction between data containing just background noise and data containing a microseismic event.

4 DISCUSSION

As shown in figures 3 and 4, the approximation method proposed here provides a large separation between events and background noise across frequencies, which is qualitatively similar to the traditional method in differentiating between the events and background noise. By studying the R matrix, we gain some insight into some properties of the background noise and event signals that help this method provide reasonable approximations. The rows and columns of the R matrix do not correspond directly to either the time or sensor component of the data although it has the dimensions 'number of sub-windows $\times$ number of sub-windows'. However, as stated previously, the i^{th} entry of the j^{th} row of the R matrix represents the magnitude of the j^{th} column of the Q matrix contained in the i^{th} column of the original matrix. Hence, we can relate the columns of R to the various sub-windows and the rows to the columns of Q.

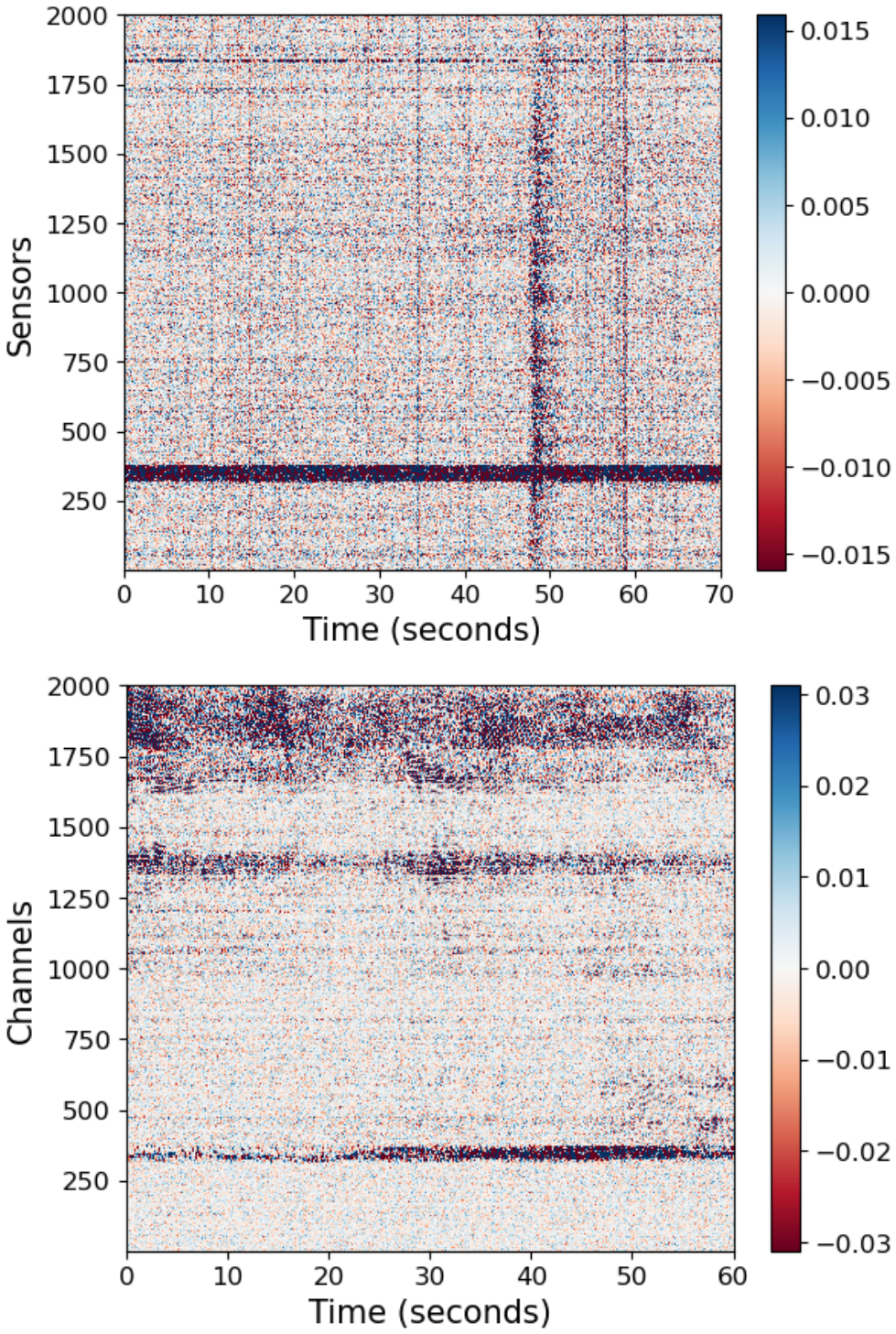

Figure 2. Data used for experiments. The data above contains three microseismic events that happen within the space of about five seconds from each other, the first of which appears at about 50 seconds. The image below shows data recorded between 12:00:18 AM and 12:01:18 AM on March 12, 2016, and is expected to contain only background noise.

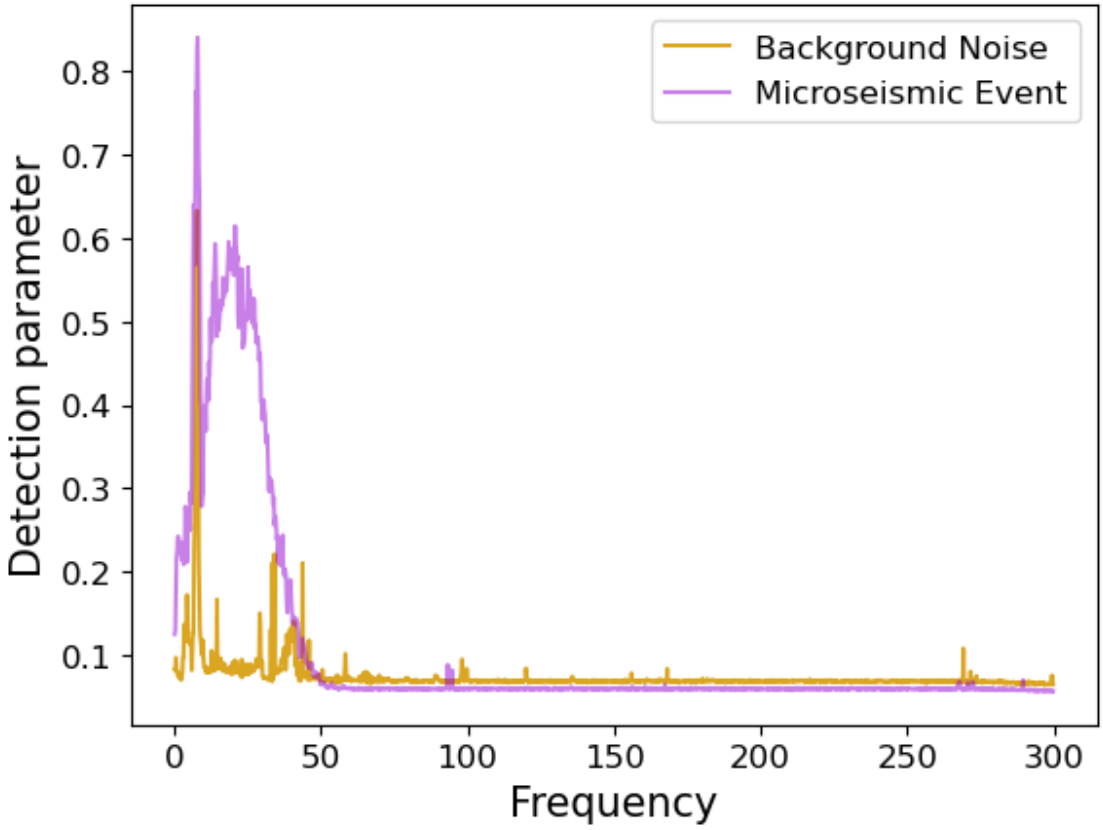

Figure 3. Detection parameter at various frequencies for microseismic activity (violet) and background noise (yellow). The detection parameter is generally low for the noise except at 7.5 Hz. That of the event shows high magnitudes in a wide frequency band below 50 Hz

First, looking at the R matrix for the 7.5 Hz noise (figure 5 (top)), we observe a prevalent presence of strong components in the direction of the first two columns of Q, as evident from the first two rows of R. In the bottom image of Figure 5, we further note that the approximate eigenvalues corresponding to the first two sub-windows significantly surpass those of others, meeting the criterion for classification as an event. On the other hand, upon inspecting the R matrix of background noise (figure 6), we do not see any row displaying notably larger values across multiple entries. This underscores the incoherence of such noise types. Consequently, we can say that one condition for the classification of events through this approximation of coherence analysis is its coherence across sub-windows.

Next, we can inspect the R matrix corresponding to the recognized event shown in Figure 7. Here, we observe low amplitudes across all entries, except for two diagonal entries corresponding to the sub-windows where the events transpire. The corresponding plot for the approximate eigenvalues reveals elevated values precisely at these locations. Since we don't see any pattern of coherence here, the simple explanation for the recognition of this event is the increase in magnitude within the frequency band of the event within the respective sub-window. This gives us an alternate condition under which some signal might be classified as an event using the algorithm provided.

5 CONCLUSIONS

We introduced an algorithm relying on QR decomposition, offering an efficient approximation of coherence-based event detection. This method effectively identifies events characterized by coherence across multiple sub-windows or transient high amplitudes. Extensions of this algorithm could involve the creation of streaming versions capable of real-time event identification. This could be particularly important for applications where a limited subset of data associated with potential microseismic events could be

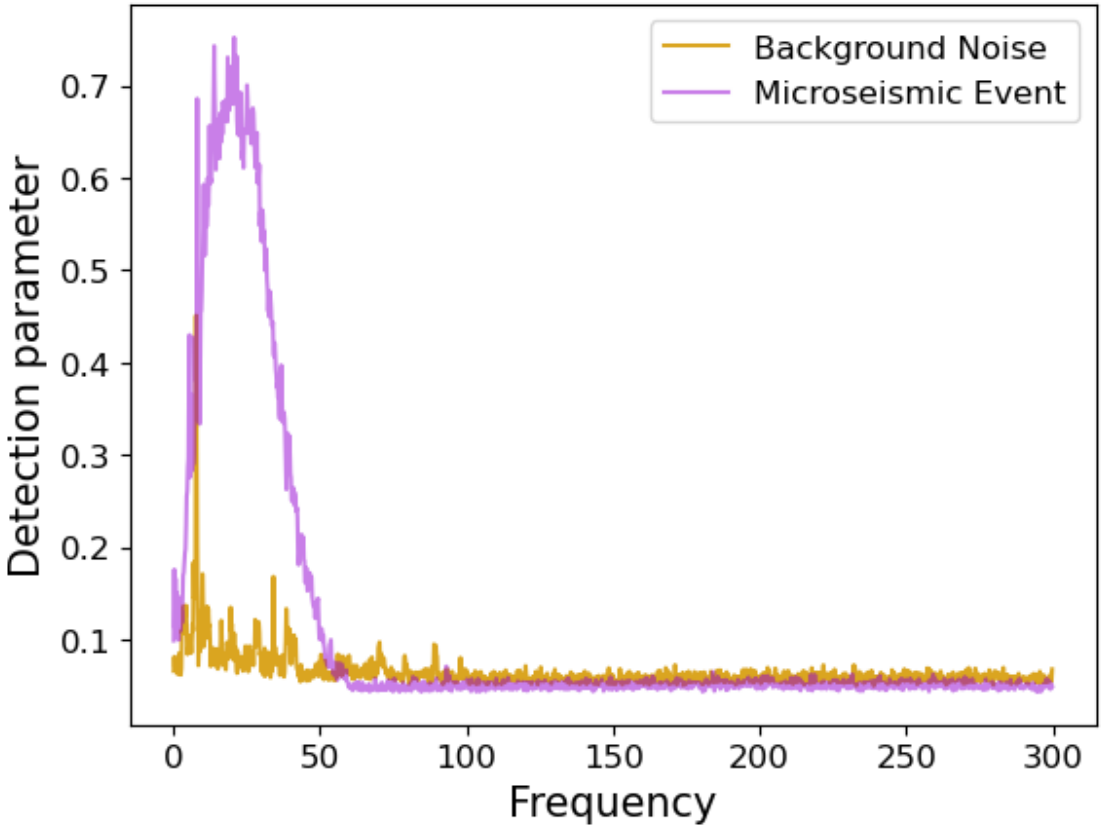

Figure 4. Detection parameter approximated with QR decomposition at various frequencies for microseismic activity (violet) and background noise (yellow). Like in the normal approach, the detection parameter is generally low for the noise except at 7.5 Hz. That of the event shows high magnitudes in a wide frequency band below 50 Hz.

telemetered from the field elsewhere for expert analysis. Another extension that is an avenue of interest lies in exploring compressed formats that can accompany this algorithm, facilitating event search within compressed versions of extensive archived data, which could provide cost reductions for the management and sharing of large DAS data archives.

6 ACKNOWLEDGEMENTS

We thank the National Science Foundation Grant 2046387, the Air Force Research Laboratory Subaward 62681767-227888 through Stanford University, and the sponsor companies of the Center for Wave Phenomena (CWP), whose support made this research possible. We also thank the students and faculty of CWP and the Martin Group for helpful discussions throughout this work.

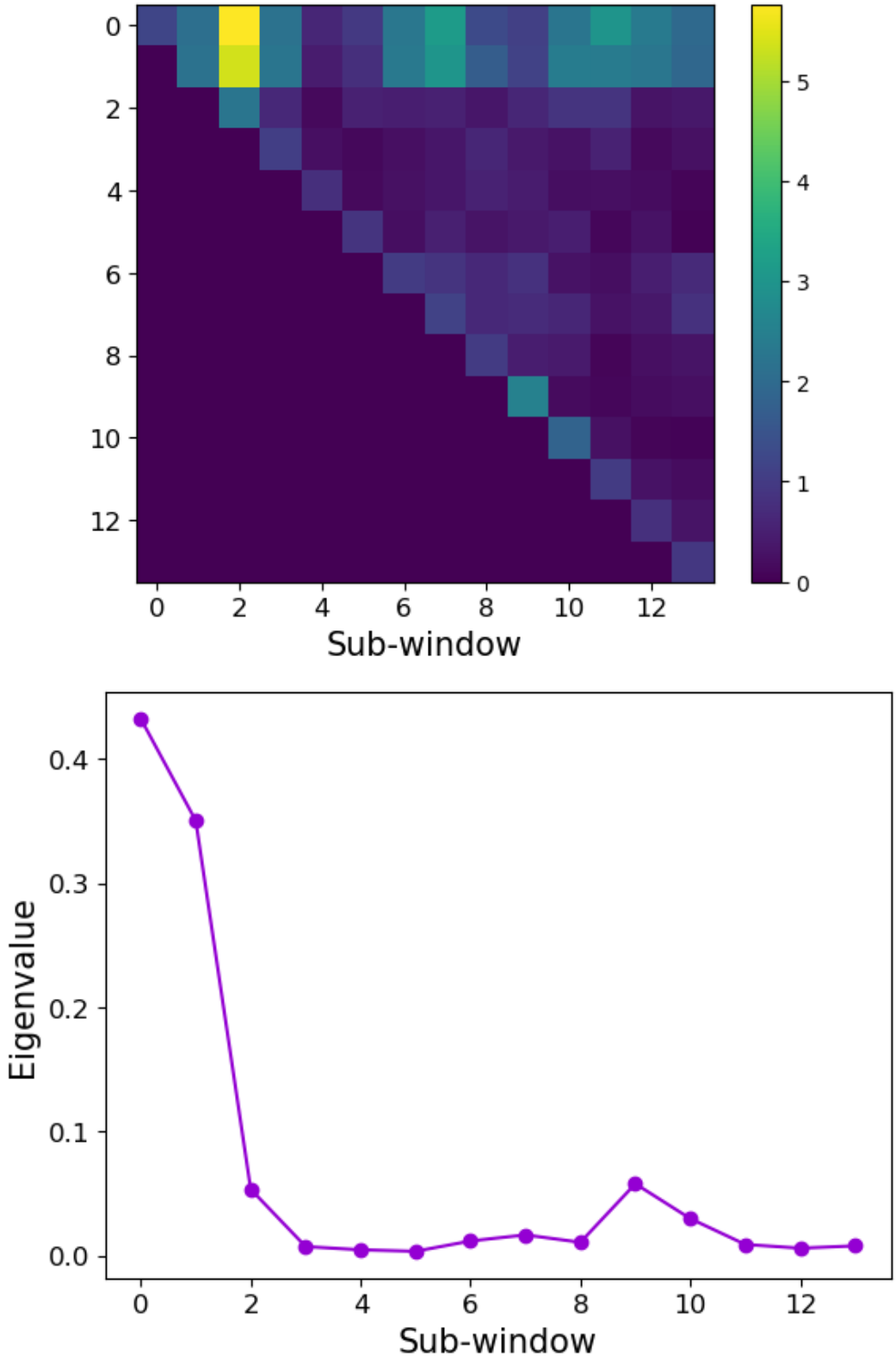

Figure 5. R matrix for the recurrent noise at 7.5Hz (top) and the corresponding "eigenvalue" approximations (bottom). The first two rows have generally high amplitude across all columns. This is an indication of the persistence of the noise in time. The approximate eigenvalues are increased in the first two entries which relate to the coherent noise and hence this is classified by the algorithm as an event.

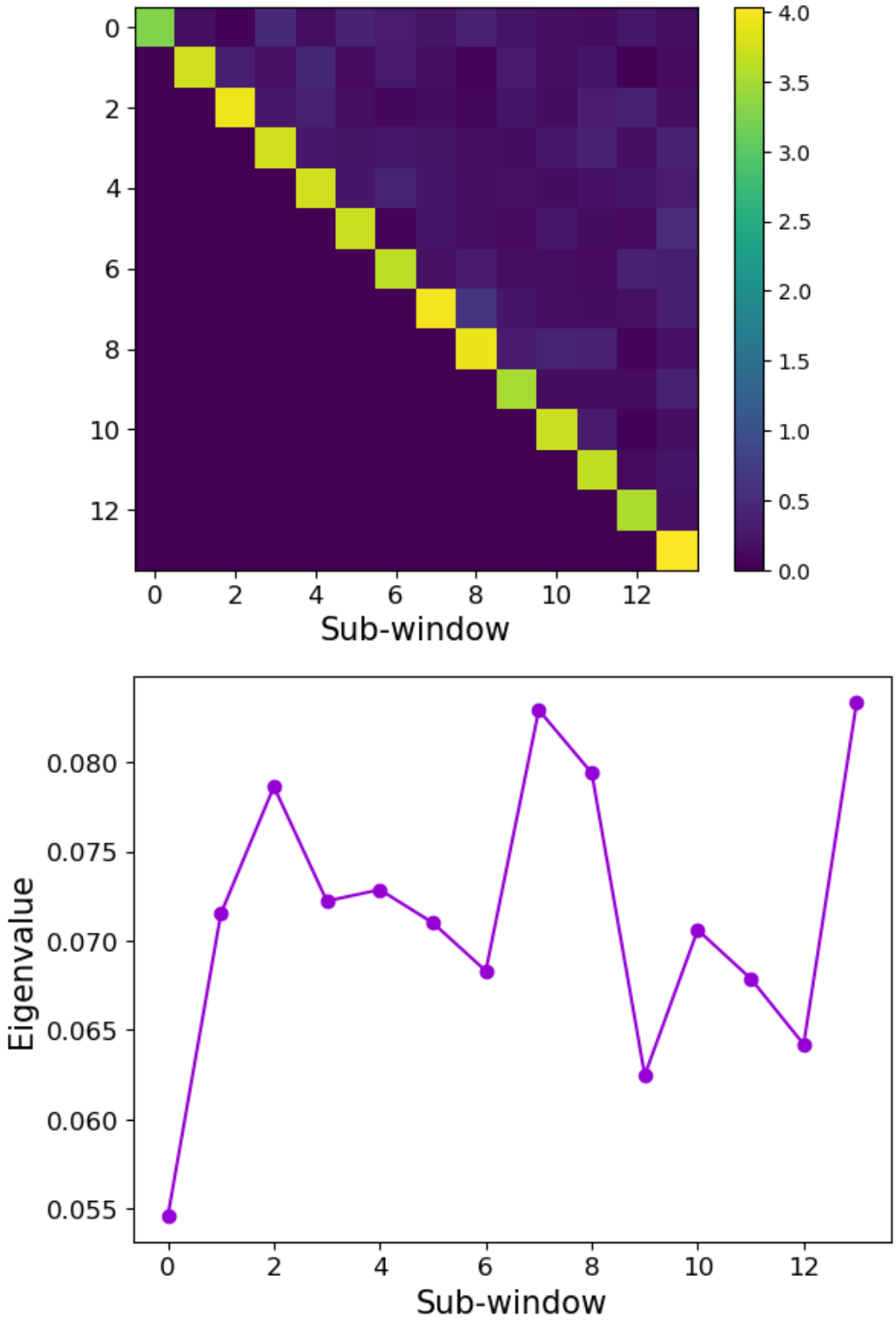

Figure 6. R matrix for the background noise (top) and the corresponding "eigenvalue" approximations (bottom). Unlike the case of the coherent noise, none of the rows in the R matrix exhibit high magnitudes across the columns. This shows the incoherence of this noise. Consequently, the eigenvalue estimates vary very little in magnitude and hence this would be classified rightly as noise.

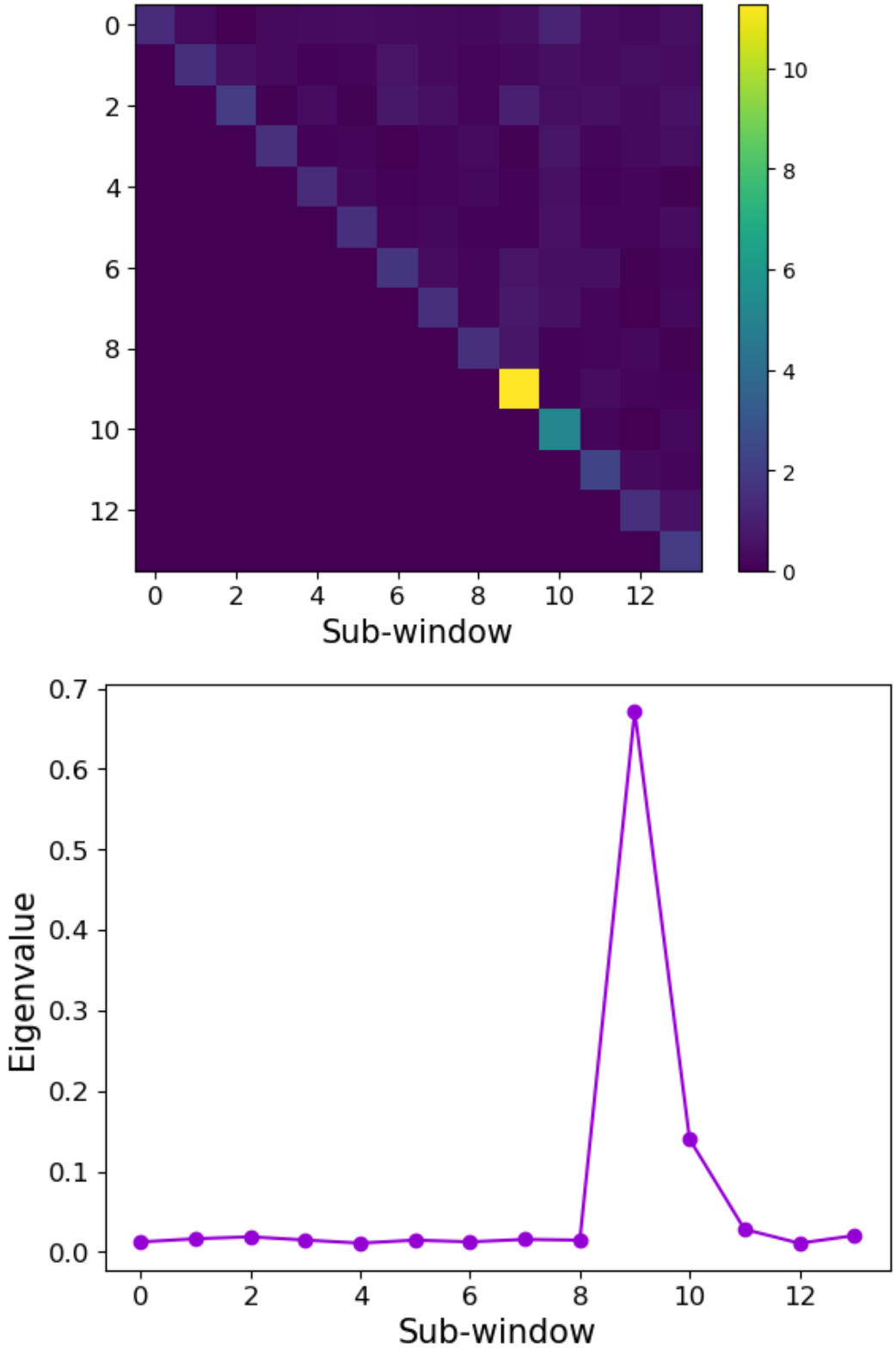

Figure 7. R matrix for the microseismic event (top) and the corresponding "eigenvalue" approximations (bottom). This shows generally low magnitude except for the columns corresponding to the sub-windows within which the events occur. We don't see much coherence here but the increase in amplitude results in a high "eigenvalue" and hence this was classified rightly as an event.

REFERENCES

Coffey, A., S. Bista, A. Fasano, T. Buxo, M. Mitchell, E. R. Giglia, S. Dukic, M. Fenech, M. Barry, A. Wade, M. Heverin, M. Muthuraman, R. G. Carson, M. Lowery, O. Hardiman, and B. Nasseroleslami, 2021, Altered supraspinal motor networks in survivors of poliomyelitis: A cortico-muscular coherence study: Clinical Neurophysiology, **132**, 106–113.

Coleman, T., 2016, Brady's Geothermal Field - Metadata for DTS and DAS Surveys.

Gibbons, S. J., and F. Ringdal, 2006, The detection of low magnitude seismic events using array-based waveform correlation: Geophysical Journal International, **165**, 149–166.

Lawley, D. N., 1956, TESTS OF SIGNIFICANCE FOR THE LATENT ROOTS OF COVARIANCE AND CORRELATION MATRICES: Biometrika, **43**, 128–136.

Li, Z., and Z. Zhan, 2018, Pushing the limit of earthquake detection with distributed acoustic sensing and template matching: a case study at the Brady geothermal field: Geophysical Journal International, **215**, 1583–1593.

Sabbione, J. I., and D. Velis, 2010, Automatic first-breaks picking: New strategies and algorithms: GEOPHYSICS, **75**, V67–V76.

Seydoux, L., N. Shapiro, J. De Rosny, F. Brenguier, and M. Landès, 2016, Detecting seismic activity with a covariance matrix analysis of data recorded on seismic arrays: Geophysical Journal International, **204**, 1430–1442.